

Entangling Higgs production associated with a single top and a top-quark pair in the presence of anomalous top-Yukawa coupling

Jung Chang¹, Kingman Cheung^{1,2,3}, Jae Sik Lee^{4,1}, and Chih-Ting Lu³

¹ *Physics Division, National Center for Theoretical Sciences, Hsinchu, Taiwan*

² *Division of Quantum Phases and Devices, School of Physics,
Konkuk University, Seoul 143-701, Republic of Korea*

³ *Department of Physics, National Tsing Hua University, Hsinchu 300, Taiwan*

⁴ *Department of Physics, Chonnam National University,
300 Yongbong-dong, Buk-gu, Gwangju, 500-757, Republic of Korea*

(Dated: July 22, 2016)

Abstract

The ATLAS and CMS collaborations observed the excess in the associated Higgs production with a top-quark pair ($t\bar{t}h$) and reported the signal strengths of $\mu_{t\bar{t}h}^{\text{ATLAS}} = 1.81 \pm 0.80$ and $\mu_{t\bar{t}h}^{\text{CMS}} = 2.75 \pm 0.99$ based on the data collected at $\sqrt{s} = 7$ and 8 TeV. In this work, we attempt to interpret the excess by exploiting the strong entanglement between the associated Higgs production with a single top quark (thX) and $t\bar{t}h$ production in the presence of anomalous top-Yukawa coupling. As well known, $t\bar{t}h$ production only depends on the absolute value of the top-Yukawa coupling. Meanwhile, in thX production, this degeneracy is lifted through the strong interference between the two main contributions which are proportional to the top-Yukawa and the gauge-Higgs couplings, respectively. Especially, when the relative sign of the top-Yukawa coupling with respect to the gauge-Higgs coupling is reversed, the thX cross section can be enhanced by more than one order of magnitude. We perform a detailed study of the influence of thX production on $t\bar{t}h$ production in the presence of the anomalous top-Yukawa coupling. While assuming the Standard Model (SM) value for the gauge-Higgs coupling, we vary the top-Yukawa coupling within the range allowed by the current LHC Higgs data. We consider the Higgs decay modes into multileptons, $b\bar{b}$ and $\gamma\gamma$ putting a particular emphasis on the same sign dilepton events. We also discuss the prospects for the LHC Run-2 on how to disentangle thX production from $t\bar{t}h$ one and how to probe the anomalous top-Yukawa coupling.

I. INTRODUCTION

The Higgs boson was discovered at the Large Hadron Collider (LHC) [1, 2]. After analyzing almost all the Run-1 data, the measured properties of the Higgs boson are the best described by the standard model (SM) Higgs boson [3], which was proposed in 1960s [4]. The most constrained is the Higgs coupling to the massive gauge bosons normalized to the corresponding SM value (gauge-Higgs couplings) $C_v = 0.94^{+0.11}_{-0.12}$, which is very close to the SM value [5]. On the other hand, the top- and bottom-Yukawa couplings cannot be determined as precisely as C_v by the current data. Currently, they are within 30 – 40% of the SM values [5], yet, the negative regime of the top-Yukawa coupling is still allowed at 95% confidence level (CL) ¹.

On the other hand, one of the most exciting results from both ATLAS and CMS in their Run-1 data was the excess in the same-sign dilepton events with b -jets and missing transverse energy [6–8]. The ATLAS collaboration reported a significance of about 2σ in the exotic search [6] and the CMS collaboration a significance of about 2.5σ in the $t\bar{t}h$ Higgs search [7]. Some people have taken them as the twilight of new physics beyond the SM [9].

In this work, we focus on the excess observed in Higgs boson production in association with a top-quark pair ($t\bar{t}h$). In the same sign dilepton channel ($ss2\ell$), the best-fit signal strengths are: $\mu_{t\bar{t}h,ss2\ell}^{\text{ATLAS}} = 2.8^{+2.1}_{-1.9}$ [10] and $\mu_{t\bar{t}h,ss2\ell}^{\text{CMS}} = 5.3^{+2.1}_{-1.8}$ [7]. The CMS excess is about 2.5σ above the SM prediction while the ATLAS result is still consistent with the SM. While, the best-fit signal strengths for combined channels are: $\mu_{t\bar{t}h}^{\text{ATLAS}} = 1.81 \pm 0.80$ and $\mu_{t\bar{t}h}^{\text{CMS}} = 2.75 \pm 0.99$ at $\sqrt{s} = 7$ and 8 TeV [5]. Here we attempt to interpret the excess by exploiting the strong entanglement between the associated Higgs production with a single top quark (thX) and $t\bar{t}h$ production in the presence of anomalous top-Yukawa coupling.

As well known $t\bar{t}h$ production only depends on the absolute value of the top-Yukawa coupling at the leading order (LO), see Fig. 1, which is similar to gluon-gluon fusion production. Therefore, the $t\bar{t}h$ cross section is insensitive to the sign of the top-Yukawa coupling at LO. Meanwhile, in thX production, this degeneracy is lifted through the strong interference between the two main contributions, which are proportional to the top-Yukawa and the gauge-Higgs couplings, respectively. Note that we include both $th+X$ and $\bar{t}h+X$ production

¹ The model-independent fit to the current Higgs data shows that, when the bottom- and tau-Yukawa couplings are allowed to vary in addition to the gauge-Higgs and top-Yukawa couplings, the negative top-Yukawa coupling is still allowed at 95% CL due to some collaborative effects from the bottom- and tau-Yukawa couplings [3].

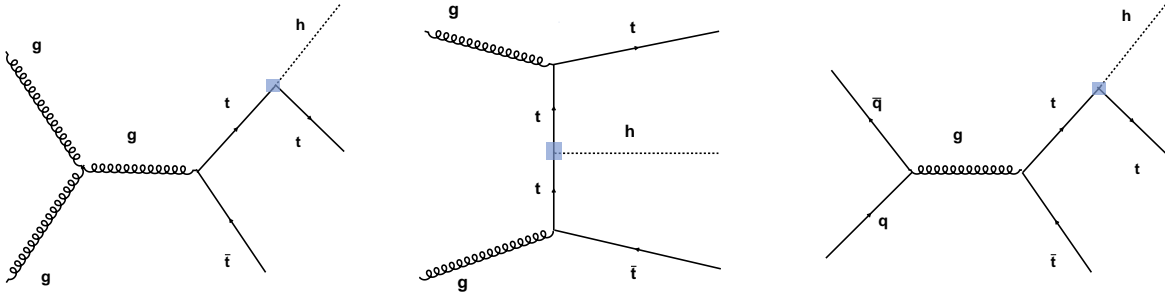


FIG. 1. Feynman diagrams contributing to $t\bar{t}h$ production at LO.

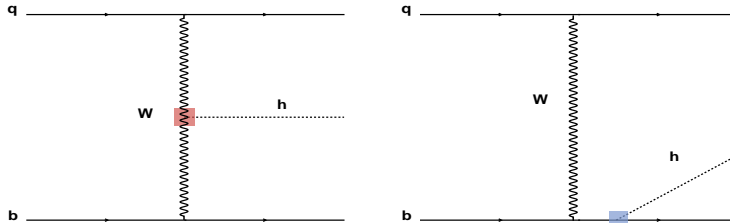


FIG. 2. Feynman diagrams contributing to thX production with $X = j$.

when we refer to thX with X denoting the accompanied particle(s) produced together with $t(\bar{t})$ and h . The Feynman diagrams contributing to thX production with $X = j$ ($qb \rightarrow thq'$) is depicted in Fig. 2. The left diagram is proportional to the gauge-Higgs coupling while the right one to the top-Yukawa coupling². The interference between the two diagrams was shown to be significant and induces large variations in the total cross section with the size and the relative sign of the Higgs couplings to the gauge bosons and the top quarks. It was shown in literature [11, 12] that the cross section can be enhanced by more than an order of magnitude when the relative sign of the top-Yukawa coupling to the gauge-Higgs coupling is reversed.

In this work, we perform a detailed study of the influence of thX production on $t\bar{t}h$ production in the presence of the anomalous top-Yukawa coupling. While assuming the Standard Model (SM) value for the gauge-Higgs coupling, we vary the top-Yukawa coupling within the allowed range by the current LHC Higgs data. We consider the Higgs decay

² We neglect the diagram with the Higgs boson attached to the bottom-quark leg which is suppressed by the small bottom-Yukawa coupling.

modes into multileptons, $b\bar{b}$ and $\gamma\gamma$ putting a particular emphasis on the same sign dilepton events. In addition to explaining the apparent excess in $t\bar{t}h$ production by entangling thX production, we also propose how to disentangle thX production from $t\bar{t}h$ one at the LHC Run-2. The main objective of this work is to further pin down the sign and the size of the top-Yukawa coupling.

The organization is as follows. In the next section, we lay down the formalism and the calculation method. In Sec. III, we show the influence of thX with the anomalous top-Yukawa coupling on $t\bar{t}h$ for both the ATLAS and CMS Run-1 data. In Sec. IV, we propose some scenarios to further disentangle thX from $t\bar{t}h$ for the LHC Run-2. Finally, we discuss and conclude in Sec. V.

II. FORMALISM

A. Processes and Higgs couplings involved

We consider two types of production processes for the Higgs boson and the top quark. The first one is the associated production of the Higgs with a pair of top quarks, see Fig. 1. The second one is the associated Higgs production with a single top quark plus anything else: thX production with $X = j (qb \rightarrow thq')$, $jb (qg \rightarrow thq'b)$, $W (gb \rightarrow thW)$ ³, see Figs. 2 – 4 in which we have marked the vertices of hWW and $ht\bar{t}$ with squares. In $t\bar{t}h$ production, the production cross section only depends on the square of the top-Yukawa coupling. However, in thX production, the cross sections depend on the size of the gauge-Higgs and top-Yukawa couplings and the relative sign between them.

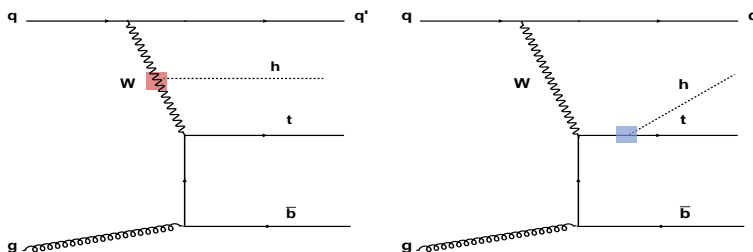


FIG. 3. Feynman diagrams contributing thX production with $X = jb$.

³ In this work, we ignore the s -channel thX process with $X = b (q\bar{q}' \rightarrow thb)$ because its production cross section is much smaller compared to other processes with $X = j, jb, W$.

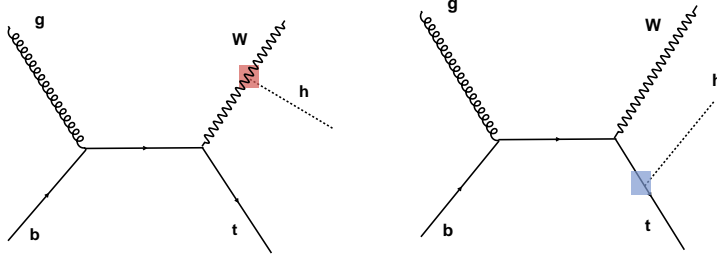


FIG. 4. Feynman diagrams contributing thX production with $X = W$.

Assuming that the Higgs boson h is a generic CP-mixed state, we can write the gauge-Higgs and Yukawa couplings as

$$\mathcal{L}_{hVV} = gm_W \left(g_{hWW} W_\mu^+ W^{-\mu} + g_{hZZ} \frac{1}{2c_W^2} Z_\mu Z^\mu \right) h, \quad (1)$$

$$\mathcal{L}_{hff} = - \sum_{f=t,b,c,\tau} \frac{gm_f}{2m_W} \bar{f} \left(g_{hff}^S + i g_{hff}^P \gamma_5 \right) f h. \quad (2)$$

Here only the gauge-Higgs coupling g_{hWW} and the top-Yukawa couplings are relevant to the $t\bar{t}h$ and thX production processes shown in Figs. 1–4. We note $g_{hWW} = g_{hZZ} = g_{hff}^S = 1$ and $g_{hff}^P = 0$ in the SM.

In order to calculate the event rates we have to consider the decay branching ratios of the Higgs boson, which depend on g_{hWW} , g_{hZZ} , $g_{htt,hbb}^{S,P}$ and a few more couplings, including $h\tau\tau$, hcc , $h\gamma\gamma$, and hgg . The amplitude for the decay process $h \rightarrow \gamma\gamma$ can be written as

$$\mathcal{M}_{h\gamma\gamma} = -\frac{\alpha m_h^2}{4\pi v} \left\{ S^\gamma(m_h) (\epsilon_{1\perp}^* \cdot \epsilon_{2\perp}^*) - P^\gamma(m_h) \frac{2}{m_h^2} \langle \epsilon_1^* \epsilon_2^* k_1 k_2 \rangle \right\}, \quad (3)$$

where $k_{1,2}$ are the momenta of the two photons and $\epsilon_{1,2}$ the wave vectors of the corresponding photons, $\epsilon_{1\perp}^\mu = \epsilon_1^\mu - 2k_1^\mu (k_2 \cdot \epsilon_1) / m_h^2$, $\epsilon_{2\perp}^\mu = \epsilon_2^\mu - 2k_2^\mu (k_1 \cdot \epsilon_2) / m_h^2$ and $\langle \epsilon_1 \epsilon_2 k_1 k_2 \rangle \equiv \epsilon_{\mu\nu\rho\sigma} \epsilon_1^\mu \epsilon_2^\nu k_1^\rho k_2^\sigma$. Retaining only the dominant loop contributions from the third-generation fermions and W^\pm , and including some additional loop contributions from new particles, the scalar and pseudoscalar form factors are given by

$$\begin{aligned} S^\gamma(m_h) &= 2 \sum_{f=b,t,\tau} N_C Q_f^2 g_{hff}^S F_{sf}(\tau_f) - g_{hWW} F_1(\tau_W) + \Delta S^\gamma, \\ P^\gamma(m_h) &= 2 \sum_{f=b,t,\tau} N_C Q_f^2 g_{hff}^P F_{pf}(\tau_f) + \Delta P^\gamma, \end{aligned} \quad (4)$$

where $\tau_x = m_h^2/4m_x^2$, $N_C = 3$ for quarks and $N_C = 1$ for tau leptons, respectively. For the loop functions of $F_{sf,pf,1}(\tau)$, we refer to, for example, Ref. [13]. The additional contributions

ΔS^γ and ΔP^γ are due to additional particles running in the loop. In the SM, $P^\gamma = 0$, $g_{hff}^S = g_{hWW} = 1$ and $\Delta S^\gamma = 0$. Similarly, the amplitude for the decay process $h \rightarrow gg$ can be written as

$$\mathcal{M}_{Hgg} = -\frac{\alpha_s m_h^2 \delta^{ab}}{4\pi v} \left\{ S^g(m_h) (\epsilon_{1\perp}^* \cdot \epsilon_{2\perp}^*) - P^g(m_h) \frac{2}{m_h^2} \langle \epsilon_1^* \epsilon_2^* k_1 k_2 \rangle \right\}, \quad (5)$$

where a and b ($a, b = 1$ to 8) are indices of the eight $SU(3)$ generators in the adjoint representation. Including some additional loop contributions from new particles, the scalar and pseudoscalar form factors are given by

$$\begin{aligned} S^g(m_h) &= \sum_{f=b,t} g_{hff}^S F_{sf}(\tau_f) + \Delta S^g, \\ P^g(m_h) &= \sum_{f=b,t} g_{hff}^P F_{pf}(\tau_f) + \Delta P^g. \end{aligned} \quad (6)$$

In the SM, $P^g = 0$, $g_{hff}^S = 1$ and $\Delta S^g = 0$. In the decays of the Higgs boson, we can see that the partial width into $b\bar{b}$ depends on g_{hbb} , that into WW^* and ZZ^* depends on $g_{hWW, hZZ}$, and that into $\gamma\gamma$ and gg depends implicitly on all g_{hWW} , $g_{htt}^{S,P}$, $g_{hbb}^{S,P}$, and $g_{h\tau\tau}^{S,P}$.

The dependence of the production cross sections and the decay branching ratios on g_{hWW} and $g_{hff}^{S,P}$ has been explicitly shown in the above equations. Since we are primarily interested in size of the gauge-Higgs and top-Yukawa couplings and the relative sign between them, for bookkeeping purpose, we use the following simplified notations

$$C_v \equiv g_{hWW} = g_{hZZ}, \quad C_t^{S,P} \equiv g_{htt}^{S,P}, \quad C_b^{S,P} \equiv g_{hbb}^{S,P}. \quad (7)$$

We shall show the anomalous top-Yukawa coupling effects on $t\bar{t}h$ and thX production at the LHC in the next section.

B. Signal strengths

First we note that signal strengths depend on the decay modes of the top quark and the Higgs boson, as well as their production mechanisms. For a choice of experimentally-defined decay mode \mathcal{D} , and taking into account the thX production processes, we define the signal strength $\mu(t\bar{t}h)$ with respect to the SM $t\bar{t}h$ production as follows

$$\mu(t\bar{t}h) = \frac{\eta_1 \sigma(t\bar{t}h) B(t\bar{t}h \rightarrow \mathcal{D}) + \sum_{X=j,b,W} \eta_X \sigma(thX) B(thX \rightarrow \mathcal{D})}{\eta_1^{\text{SM}} \sigma(t\bar{t}h)_{\text{SM}} B(t\bar{t}h \rightarrow \mathcal{D})_{\text{SM}}}, \quad (8)$$

where $\sigma(t\bar{t}h) = \sigma(pp \rightarrow t\bar{t}h)$ and $\sigma(thX) = \sigma(pp \rightarrow thX) + \sigma(pp \rightarrow \bar{t}hX)$ are understood. The detection efficiencies η 's depend on the experimental apparatuses and cuts for the specific production and decay mode. By introducing the cross-section ratios

$$\begin{aligned} R(t\bar{t}h) &\equiv \frac{\sigma(t\bar{t}h)}{\sigma(t\bar{t}h)_{\text{SM}}}, & R(thj) &\equiv \frac{\sigma(thj)}{\sigma(t\bar{t}h)_{\text{SM}}}, \\ R(thjb) &\equiv \frac{\sigma(thjb)}{\sigma(t\bar{t}h)_{\text{SM}}}, & R(thW) &\equiv \frac{\sigma(thW)}{\sigma(t\bar{t}h)_{\text{SM}}}, \end{aligned} \quad (9)$$

and the \mathcal{D} -dependent detection-efficiency ratios

$$\begin{aligned} \epsilon_1 &\equiv \frac{\eta_1 B(t\bar{t}h \rightarrow \mathcal{D})}{\eta_1^{\text{SM}} B(t\bar{t}h \rightarrow \mathcal{D})_{\text{SM}}}, & \epsilon_2 &\equiv \frac{\eta_j B(thj \rightarrow \mathcal{D})}{\eta_1^{\text{SM}} B(t\bar{t}h \rightarrow \mathcal{D})_{\text{SM}}}, \\ \epsilon_3 &\equiv \frac{\eta_{jb} B(thjb \rightarrow \mathcal{D})}{\eta_1^{\text{SM}} B(t\bar{t}h \rightarrow \mathcal{D})_{\text{SM}}}, & \epsilon_4 &\equiv \frac{\eta_W B(thW \rightarrow \mathcal{D})}{\eta_1^{\text{SM}} B(t\bar{t}h \rightarrow \mathcal{D})_{\text{SM}}}, \end{aligned} \quad (10)$$

one may have

$$\mu(t\bar{t}h) = \epsilon_1 R(t\bar{t}h) + \epsilon_2 R(thj) + \epsilon_3 R(thjb) + \epsilon_4 R(thW). \quad (11)$$

We note that $\epsilon_1 = R(t\bar{t}h) = 1$ in the SM limit of $C_v = 1$, $C_t^S = +1$, and $C_t^P = 0$ and $\mu(t\bar{t}h)$ is always larger than 1 due to the entanglement of thX production. Our main task is to calculate the cross section ratios R 's in the presence of anomalous top-Yukawa coupling and the detection-efficiency ratios $\epsilon_{1,2,3,4}$ for various top-quark and Higgs-boson decay modes.

III. thX PRODUCTION WITH THE ANOMALOUS TOP-YUKAWA COUPLING

Both the CMS [7] and ATLAS [10, 14, 15] collaborations have published the results of their searches for the associated production of the Higgs boson with a top-quark pair via different Higgs decay channels at $\sqrt{s} = 7$ and 8 TeV. We summarize their best-fit results in Table I. Since the experimental uncertainties in the hadronically-decaying τ and 4ℓ categories are too large at this stage, we shall focus only on the $ss2\ell$, 3ℓ , $\gamma\gamma$ and $b\bar{b}$ categories in our analysis below. In the $\gamma\gamma$ category for $h \rightarrow \gamma\gamma$, both CMS [7] and ATLAS [14] included all the decay modes of a top-quark pair: semileptonic ($t\bar{t} \rightarrow \nu j j b b$), leptonic ($t\bar{t} \rightarrow \nu l \nu l b b$), and hadronic ($t\bar{t} \rightarrow j j j j b b$) modes. On the other hand, in the $b\bar{b}$ category for $h \rightarrow b\bar{b}$, both CMS [7] and ATLAS [15] considered only the semileptonic and leptonic decay modes of the top-quark pair. Finally, in the categories of $ss2\ell$ and 3ℓ for $h \rightarrow$ multileptons, both CMS [7] and ATLAS [10] included only the semileptonic decay mode of the top-quark pair.

TABLE I. The best-fit values for the category-dependent signal strengths $\mu_{t\bar{t}h}^{\text{CMS}}$ and $\mu_{t\bar{t}h}^{\text{ATLAS}}$ coming from the CMS [7] and ATLAS [10][14][15] searches, respectively, for the associated production of the Higgs boson with a top quark pair at $\sqrt{s}=7$ and 8 TeV for $m_h = 125.6$ GeV (CMS) / 125 GeV (ATLAS).

Category	CMS $t\bar{t}h$ channel	ATLAS $t\bar{t}h$ channel
	$\mu_{t\bar{t}h}^{\text{CMS}}$	$\mu_{t\bar{t}h}^{\text{ATLAS}}$
$\gamma\gamma$	$+2.7^{+2.6}_{-1.8}$	$+1.3^{+3.3}_{-2.1}$
$b\bar{b}$	$+0.7^{+1.9}_{-1.9}$	$+1.5^{+1.1}_{-1.1}$
$\tau_h\tau_h$	$-1.3^{+6.3}_{-5.5}$	–
$2\ell 1\tau_h$	–	$-0.9^{+3.1}_{-2.0}$
$1\ell 2\tau_h$	–	$-9.6^{+9.6}_{-9.7}$
4ℓ	$-4.7^{+5.0}_{-1.3}$	$+1.8^{+6.9}_{-2.0}$
3ℓ	$+3.1^{+2.4}_{-2.0}$	$+2.8^{+2.2}_{-1.8}$
$ss2\ell$	$+5.3^{+2.1}_{-1.8}$	$+2.8^{+2.1}_{-1.9}$

In order to perform a detailed study of the influence of thX production with anomalous top-Yukawa coupling on $t\bar{t}h$ production, we simulate both the thX and $t\bar{t}h$ processes and generate events by MadGraph5 [16], perform parton showering and hadronization by Pythia 8.1 [17], and employ the detector simulations by Delphes 3 [18]. We use NN23LO1 for parton distribution functions with different renormalization/factorization scales which we shall show below. We follow the selection cuts and detector efficiencies of the CMS [7] and ATLAS [10, 14, 15] $t\bar{t}h$ searches. We summarize the signatures of the search channels used in the $t\bar{t}h$ analysis for CMS in Table II and for ATLAS in Table III.

We calculate the $t\bar{t}h$ production cross section with the factorization (μ_F) and renormalization (μ_R) scales set at $m_t + m_h/2$ in the four-flavor scheme. On the other hand, in computing the production cross sections for thX , we include the t -channel thj and $thjb$ processes and the thW process, but ignore the s -channel thb process due to its much smaller cross section. In calculating the production cross sections for thj ($thjb$), $\mu_F = \mu_R$ are set at 75 GeV in the five-flavor (four-flavor) scheme. For thW , we are employing the dynamic factorization and renormalization scales in the five-flavor scheme.

TABLE II. The signature of the search channels used in the $t\bar{t}h$ analysis for the CMS.

Category	$t\bar{t}h$ decay modes	Signature	Background
$h \rightarrow b\bar{b}$	Semileptonic $(t\bar{t}h \rightarrow l\nu jjbbbb)$	1 e/μ , $P_T > 30$ GeV ≥ 4 jets + ≥ 2 b-tags, $P_T > 30$ GeV	$t\bar{t}$ + jets $t\bar{t} + W/Z$
	Leptonic $(t\bar{t}h \rightarrow l\nu l\nu bbbb)$	1 e/μ , $P_T > 20$ GeV 1 e/μ , $P_T > 10$ GeV ≥ 3 jets + ≥ 2 b-tags, $P_T > 30$ GeV	Single t W/Z +jets Diboson
	Semileptonic $(t\bar{t}h \rightarrow l\nu jjbb\gamma\gamma)$	2 γ , $P_T > m_{\gamma\gamma}/2$ (25) GeV for 1 st (2 nd) ≥ 1 e/μ , $P_T > 20$ GeV	$t\bar{t}$ + jets $t\bar{t} + W/Z$
	Leptonic $(t\bar{t}h \rightarrow l\nu l\nu bb\gamma\gamma)$	≥ 2 jets + ≥ 1 b-tags, $P_T > 25$ GeV	Single t
$h \rightarrow \gamma\gamma$	Hadronic $(t\bar{t}h \rightarrow jjjjbb\gamma\gamma)$	2 γ , $P_T > m_{\gamma\gamma}/2$ (25) GeV for 1 st (2 nd) 0 e/μ , $P_T > 20$ GeV ≥ 4 jets + ≥ 1 b-tags, $P_T > 25$ GeV	$t\bar{t}$ + jets $t\bar{t} + W/Z$ Single t
$h \rightarrow$ Leptons	Same-Sign Dilepton $(t\bar{t}h \rightarrow l^\pm \nu l^\pm [\nu] jjj[j]bb)$	2 e/μ , $P_T > 20$ GeV ≥ 4 jets + ≥ 1 b-tags, $P_T > 25$ GeV	$t\bar{t}W$ $t\bar{t}Z/\gamma^*$
$h \rightarrow WW$			
$h \rightarrow \tau\tau$	3 Leptons $(t\bar{t}h \rightarrow l\nu[l\nu]l[\nu]j[j]bb)$	1 e/μ , $P_T > 20$ GeV 1 e/μ , $P_T > 10$ GeV 1 $e(\mu)$, $P_T > 7(5)$ GeV ≥ 2 jets + ≥ 1 b-tags, $P_T > 25$ GeV	$t\bar{t}WW$ $t\bar{t}\gamma$ WZ ZZ
$h \rightarrow ZZ$			

As shown in Refs. [3] in which the model-independent fit to the current Higgs data is performed, the negative $C_t^S = -1$ is ruled at 95%CL if only the gauge-Higgs coupling C_v and the top-Yukawa coupling C_t^S vary. However, $C_t^S = -1$ is still allowed at 95%CL when the gauge-Higgs C_v , top-Yukawa C_t^S , bottom-Yukawa C_b^S , and tau-Yukawa C_τ^S couplings are all allowed to vary. Furthermore, if some sizable contributions to ΔS^γ and ΔS^g due to additional new particles running in the loop are assumed, a broad range of C_t^S between -2 and $+2$ is still consistent with the current Higgs data.

In the following, we show the results of our numerical analysis in each of categories of Leptons ($ss2\ell$ and 3ℓ), $\gamma\gamma$, and $b\bar{b}$ for the Higgs boson decaying into multileptons, two

TABLE III. The signature of the search channels used in the $t\bar{t}h$ analysis for the ATLAS.

Category	$t\bar{t}h$ decay modes	Signature	Background
$h \rightarrow b\bar{b}$	Semileptonic ($t\bar{t}h \rightarrow l\nu jj bbb$)	$1 e/\mu, P_T > 25 \text{ GeV}, \Delta R < 0.15$ $\geq 4 \text{ jets} + \geq 2\text{b-tags}$	$t\bar{t}$ +jets $t\bar{t} + V$
	Leptonic ($t\bar{t}h \rightarrow l\nu l\nu bbb$)	$1 e/\mu, P_T > 25 \text{ GeV}$ $1 e/\mu, P_T > 15 \text{ GeV}$ $\geq 2\text{b-tags}$	V +jets ($V = W, Z$)
$h \rightarrow \gamma\gamma$	Semileptonic ($t\bar{t}h \rightarrow l\nu jj bb\gamma\gamma$)	$2\gamma, E_T > 0.35(0.25) \times m_{\gamma\gamma}$ for $1^{st}(2^{nd})$ $\geq 1 e/\mu, E_T(e) > 15 \text{ GeV}, P_T(\mu) > 10 \text{ GeV}$	
	Leptonic ($t\bar{t}h \rightarrow l\nu l\nu bb\gamma\gamma$)	$\geq 1 \text{ b-tags}$	
	Hadronic ($t\bar{t}h \rightarrow jjjj bb\gamma\gamma$)	$2\gamma, E_T > 0.35(0.25) \times m_{\gamma\gamma}$ for $1^{st}(2^{nd})$ $0 e/\mu$ $\geq 5 \text{ jets} + \geq 1 \text{ b-tags}, P_T > 25 \text{ GeV}$	
$h \rightarrow \mathbf{Leptons}$	Same-Sign Dilepton ($t\bar{t}h \rightarrow l^\pm \nu l^\pm [\nu] jjj [j] bb$)	(sub)leading lepton : $2 e/\mu, P_T > 25(20) \text{ GeV}$ $\geq 4 \text{ jets} + \geq 1\text{b-tags}, P_T > 25 \text{ GeV}$	$t\bar{t}$ +jets $t\bar{t} + V$
$h \rightarrow WW$	3 Leptons ($t\bar{t}h \rightarrow l\nu l[\nu] l[\nu] j[j] bb$)	$1 e/\mu, P_T > 25 \text{ GeV}$	Diboson
$h \rightarrow \tau\tau$		$1 e/\mu, P_T > 20 \text{ GeV}$	
$h \rightarrow ZZ$		$1 e/\mu, P_T > 10 \text{ GeV}$	
		$\geq 4 \text{ jets} + \geq 1 \text{ b-tags}, P_T > 25 \text{ GeV}$ (or $3 \text{ jets} + \geq 2 \text{ b-tags}, P_T > 25 \text{ GeV}$)	

photons, and two b quarks, respectively. Note that, in our numerical analysis, we vary the top-Yukawa coupling C_t^S within the range allowed by the current LHC Higgs data while taking the SM value for the gauge-Higgs coupling, $C_v = 1$. For the bottom-Yukawa C_b^S and tau-Yukawa C_τ^S couplings, one may freely take either $+1$ or -1 since their signs would have negligible effects on the production cross sections and decay branching ratios. Finally, all the CP-odd Yukawa couplings are supposed to vanish, $C_{t,b,\tau}^P = 0$.

A. Category Leptons for $h \rightarrow$ multileptons

In the category Leptons which includes leptonic decays of $h \rightarrow WW, ZZ, \tau\tau \rightarrow$ multileptons, we focus on the subcategories of $ss2\ell$ and 3ℓ modes. We shall use several different values of C_t^S to show the possibly strong entanglement between thX production and $t\bar{t}h$ production for both the ATLAS and CMS analyses. Note that CMS used the so-called Multivariate Analysis (MVA) method in their analysis, however, we only follow their set of preselection cuts and event selection requirements to perform the cut-based analysis.

First, we note that the CMS and ATLAS collaborations were adopting different signatures and preselection cuts to analyze the category Leptons as shown in Table II and Table III ⁴. The CMS analysis was performed in the $ss2\ell$ and 3ℓ subcategories while the ATLAS analysis was carried out in the subcategories of $2\ell + 4j$, $2\ell + \geq 5j$, and 3ℓ . Without knowing an appropriate way to combine the two sets of data, we present our results handling the CMS and ATLAS cases separately to make full use of the existing data. Further, in the CMS and ATLAS analyses of the 3ℓ subcategory, also required was a low-mass invariant-mass cut $M_{\ell\ell} > 12$ GeV to remove the J/Ψ background and a Z -pole mass veto cut $|M_{\ell+\ell-} - M_Z| > 10$ GeV to suppress the Z background. Some additional cuts on the scalar sum of the transverse momenta (P_T) of the two leptons and the missing energy (E_T^{miss}) were also applied in the CMS case.

To quantify the effects of different values of C_t^S on $t\bar{t}h$ and thX , we use the signal-strength formula for $\mu(t\bar{t}h)$ in Eq. (8), which consists of the sum of the products of the cross section ratios R 's and the \mathcal{D} -dependent detection efficiency ratio ϵ 's, which are in turns given by Eq. (9) and Eq. (10), respectively. Explicitly, we have

$$\begin{aligned} \mu(t\bar{t}h) &= \frac{\sigma(t\bar{t}h)_{C_t^S}}{\sigma(t\bar{t}h)_{SM}} \times \epsilon_1 + \frac{\sigma(thj)_{C_t^S}}{\sigma(t\bar{t}h)_{SM}} \times \epsilon_2 + \frac{\sigma(thjb)_{C_t^S}}{\sigma(t\bar{t}h)_{SM}} \times \epsilon_3 + \frac{\sigma(thW)_{C_t^S}}{\sigma(t\bar{t}h)_{SM}} \times \epsilon_4 \\ &= R(t\bar{t}h) \times \epsilon_1 + R(thj) \times \epsilon_2 + R(thjb) \times \epsilon_3 + R(thW) \times \epsilon_4. \end{aligned} \quad (12)$$

In Table IV, we show the cross sections ratios $R(t\bar{t}h)$ and $R(thX)$ with $X = j, jb, W$ at the 8 TeV LHC (LHC-8) taking $C_t^S = \pm 1$ and ± 1.5 . Note $R(t\bar{t}h) = 1$ (2.25) for $|C_t^S| = 1$ (1.5) and the thX cross sections can be largely enhanced for the negative values of C_t^S .

In Table V, we show the \mathcal{D} -dependent detection efficiency ratios $\epsilon_{1,2,3,4}$ with the CMS cuts in the $ss2\ell$ (upper) and 3ℓ (lower) subcategories for $C_t^S = \pm 1, \pm 1.5$. By using the

⁴ This is true also for the $\gamma\gamma$ and $b\bar{b}$ categories.

TABLE IV. The cross-section ratios $R(t\bar{t}h)$ and $R(thX)$ with $X = j, jb, W$ defined in Eq. (9). We are taking $\sqrt{s} = 8$ TeV (LHC-8) and $C_t^S = \pm 1, \pm 1.5$.

LHC-8	$C_t^S = 1$	$C_t^S = -1$	$C_t^S = 1.5$	$C_t^S = -1.5$
Cross Section of $t\bar{t}h$ (pb)	0.13			
$R(t\bar{t}h)$	1	1	2.25	2.25
$R(thj)$	0.16	1.86	0.30	2.82
$R(thjb)$	4.77e-2	0.59	9.39e-2	0.93
$R(thW)$	3.21e-2	0.19	7.05e-2	0.31

cross section ratios given in Table IV, one can obtain the CMS $t\bar{t}h$ signal strengths $\mu_{t\bar{t}h}^{\text{CMS}}$. We observe that $\mu_{t\bar{t}h,ss2\ell}^{\text{CMS}} > 2(3)$ for $C_t^S = 1.5(-1.5)$ and the signal strengths are larger for the negative values of C_t^S . One may make similar observations for $\mu_{t\bar{t}h,3\ell}^{\text{CMS}}$. Recently, the CMS collaboration has also reported a possible excess in the decay process $h \rightarrow \tau^\mp \mu^\pm$, $B(h \rightarrow \tau^\mp \mu^\pm) = 0.84_{-0.37}^{+0.39}\%$, with a significance of 2.4σ in the search for the lepton-flavor violation (LFV)[19]. If we take into account this LFV decay of the Higgs boson, we can slightly enhance the production rate of $h \rightarrow$ multileptons mode by a few percents. We estimate the $h \rightarrow \tau^\mp \mu^\pm$ contribution by rescaling $h \rightarrow \tau^+ \tau^-$ channel with the branching ratios and the τ detection efficiency. The CMS $t\bar{t}h$ signal strengths $\mu_{t\bar{t}h}^{\text{CMS}}$ after taking account of $h \rightarrow \tau^\mp \mu^\pm$ are also presented in Table V.

Similarly, we calculate the \mathcal{D} -dependent detection efficiency ratios $\epsilon_{1,2,3,4}$ with the ATLAS cuts in the $2\ell + 4j$ (upper), $2\ell + \geq 5j$ (middle), and 3ℓ (lower) subcategories for several values of C_t^S and present them in Table VI, together with the ATLAS $t\bar{t}h$ signal strengths $\mu_{t\bar{t}h}^{\text{ATLAS}}$. Similar observations can be made as in the CMS case.

Finally, we show in Fig. 5 the accumulative signal strengths $\mu_{t\bar{t}h,ss2\ell}^{\text{ATLAS}}$ (upper left), $\mu_{t\bar{t}h,3\ell}^{\text{ATLAS}}$ (upper right), $\mu_{t\bar{t}h,ss2\ell}^{\text{CMS}}$ (lower left), and $\mu_{t\bar{t}h,3\ell}^{\text{CMS}}$ (lower right) at $\sqrt{s} = 8$ TeV by stacking the various thX contributions on the $t\bar{t}h$ one for $C_t^S = +1, -1, +1.5, -1.5$ from left to right. The grey columns in the center without C_t^S value represent the current 8 TeV LHC data, see Table I. The ATLAS $ss2\ell$ signal strength $\mu_{t\bar{t}h,ss2\ell}^{\text{ATLAS}}$ is obtained by counting the event rates by combining the $2\ell + 4j$ and $2\ell + \geq 5j$ selections.

TABLE V. Category Leptons: The \mathcal{D} -dependent detection efficiency ratios ϵ_i 's defined in Eq. (10) with the CMS cuts for the category Leptons taking $C_t^S = \pm 1, \pm 1.5$ and $\sqrt{s} = 8$ TeV. The resulting signal strengths $\mu_{t\bar{t}h,ss2\ell}^{\text{CMS}}$ and $\mu_{t\bar{t}h,3\ell}^{\text{CMS}}$ are also shown. The last row in each partition shows the values of $\mu_{t\bar{t}h,ss2\ell}^{\text{CMS}}$ and $\mu_{t\bar{t}h,3\ell}^{\text{CMS}}$ including the contributions from $h \rightarrow \mu^\pm \tau^\mp$.

LHC-8	With CMS Analysis Cuts			
	$C_t^S = 1$	$C_t^S = -1$	$C_t^S = 1.5$	$C_t^S = -1.5$
The category of $ss2\ell$				
Efficiency of $t\bar{t}h$	9.02e-4			
ϵ_1	1	0.95	0.98	0.97
ϵ_2	0.1	0.12	0.12	0.13
ϵ_3	0.35	0.38	0.33	0.39
ϵ_4	0.68	0.85	0.72	0.83
$\mu_{t\bar{t}h,ss2\ell}^{\text{CMS}}$	1.06	1.56	2.32	3.19
$\mu_{t\bar{t}h,ss2\ell}^{\text{CMS}}$ including $h \rightarrow \tau^\mp \mu^\pm$	1.10	1.63	2.42	3.33
The category of 3ℓ				
Efficiency of $t\bar{t}h$	9.54e-4			
ϵ_1	1	0.95	1	0.97
ϵ_2	0.34	0.40	0.37	0.42
ϵ_3	0.55	0.61	0.57	0.65
ϵ_4	0.90	1.14	0.98	1.13
$\mu_{t\bar{t}h,3\ell}^{\text{CMS}}$	1.11	2.28	2.47	4.33
$\mu_{t\bar{t}h,3\ell}^{\text{CMS}}$ including $h \rightarrow \tau^\mp \mu^\pm$	1.15	2.37	2.57	4.51

B. Category $\gamma\gamma$ for $h \rightarrow \gamma\gamma$

In the category $\gamma\gamma$ for $h \rightarrow \gamma\gamma$, we include all the decay modes of the top-quark pair. We consider two subcategories of *leptonic selection* and *hadronic selection*. The lepton-selection subcategory is for the semileptonically and leptonically decaying top-quark pair while the hadronic-selection one for the hadronically decaying top-quark pair. We have also taken into account the effect of anomalous top-Yukawa coupling on the decay branching ratio

TABLE VI. Category Leptons: The same as Table V but with the ATLAS cuts.

LHC-8	With ATLAS Analysis Cuts			
	$C_t^S = 1$	$C_t^S = -1$	$C_t^S = 1.5$	$C_t^S = -1.5$
The category of $2\ell + 4j$				
Efficiency of $t\bar{t}h$	4.27e-4			
ϵ_1	1	1.05	0.96	1.0
ϵ_2	0.31	0.31	0.32	0.38
ϵ_3	0.52	0.63	0.53	0.57
ϵ_4	1.10	1.16	1.09	1.18
$\mu_{t\bar{t}h, 2\ell+4j}^{\text{ATLAS}}$	1.11	2.23	2.38	4.22
$\mu_{t\bar{t}h, 2\ell+4j}^{\text{ATLAS}}$ including $h \rightarrow \tau^\mp \mu^\pm$	1.15	2.32	2.47	4.38
The category of $2\ell + \geq 5j$				
Efficiency of $t\bar{t}h$	5.25e-4			
ϵ_1	1	0.92	0.91	0.93
ϵ_2	0.08	0.08	0.09	0.09
ϵ_3	0.25	0.28	0.22	0.26
ϵ_4	0.74	0.94	0.75	0.95
$\mu_{t\bar{t}h, 2\ell+\geq 5j}^{\text{ATLAS}}$	1.05	1.43	2.14	2.88
$\mu_{t\bar{t}h, 2\ell+\geq 5j}^{\text{ATLAS}}$ including $h \rightarrow \tau^\mp \mu^\pm$	1.09	1.48	2.23	2.99
The category of 3ℓ				
Efficiency of $t\bar{t}h$	1.05e-4			
ϵ_1	1	0.89	0.83	0.90
ϵ_2	0.06	0.09	0.13	0.09
ϵ_3	0.34	0.45	0.30	0.47
ϵ_4	0.89	1.5	0.92	1.61
$\mu_{t\bar{t}h, 3\ell}^{\text{ATLAS}}$	1.05	1.61	1.99	3.23
$\mu_{t\bar{t}h, 3\ell}^{\text{ATLAS}}$ including $h \rightarrow \tau^\mp \mu^\pm$	1.09	1.67	2.07	3.35

$B(h \rightarrow \gamma\gamma)$ ⁵.

⁵ We have $B(h \rightarrow \gamma\gamma) = (2.3, 5.4, 1.53, 5.68) \times 10^{-3}$ for $C_t^S = (1, -1, 1.5, -1.5)$ using HDECAY [20].

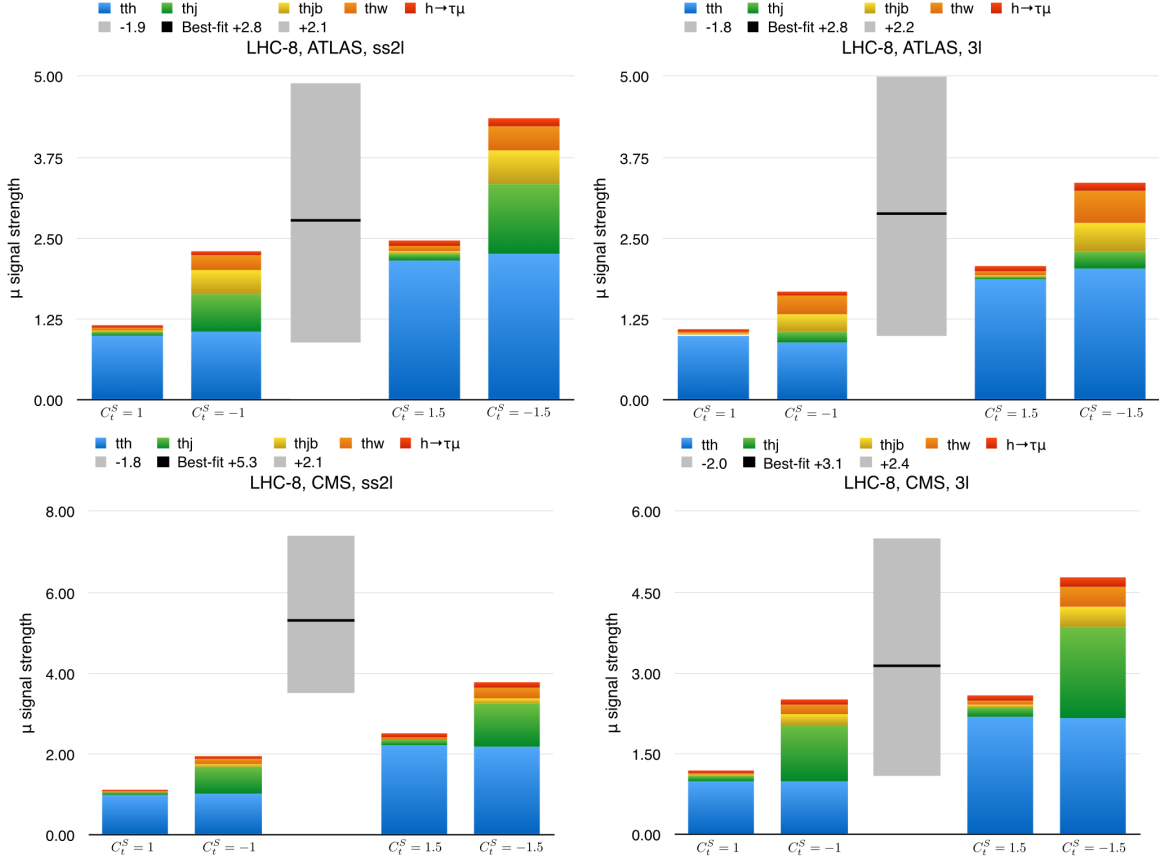


FIG. 5. Category Leptons: Accumulated signal strengths $\mu_{t\bar{t}h,ss2\ell}^{\text{ATLAS}}$ (upper left), $\mu_{t\bar{t}h,3\ell}^{\text{ATLAS}}$ (upper right), $\mu_{t\bar{t}h,ss2\ell}^{\text{CMS}}$ (lower left), and $\mu_{t\bar{t}h,3\ell}^{\text{CMS}}$ (lower right) at LHC-8 obtained by stacking the various thX contributions on the $t\bar{t}h$ one for $C_t^S = +1, -1, +1.5, -1.5$ from left to right. The grey columns in the center represent the current 8 TeV LHC data from Table I.

To repeat the CMS analysis, we follow their selection cuts listed in Table II, which are used in the cut-based analysis [7]. Also, we further impose the Higgs-mass window cut: $100 \text{ GeV} \leq m_{\gamma\gamma} \leq 180 \text{ GeV}$.

For the ATLAS analysis, we follow Ref. [14] with preselection cuts listed in Table III. We further impose the Higgs-mass window cut ($105 \text{ GeV} < m_{\gamma\gamma} < 160 \text{ GeV}$) and the ΔR cuts: $\Delta R_{l\gamma} > 0.4$, $\Delta R_{j\gamma} > 0.4$, $\Delta R_{j\mu} > 0.4$, $\Delta R_{je} > 0.2$. The missing energy cut $E_T^{\text{miss}} > 20 \text{ GeV}$ and the $e\gamma$ invariant-mass cut $M_{e\gamma} > 94 \text{ GeV}$ or $< 84 \text{ GeV}$ are also applied in the leptonic-selection category. In the hadronic-selection subcategory, we adopt the selection 1 in Ref. [14] using the working point with efficiency of 70% for identifying b -jets.

Before we present the results of our numerical study of the effects of thX on $t\bar{t}h$ in

TABLE VII. Category $\gamma\gamma$: The \mathcal{D} -dependent detection efficiency ratios ϵ_i 's defined in Eq. (10) with the CMS cuts for the category $\gamma\gamma$ taking $C_t^S = \pm 1, \pm 1.5$ and $\sqrt{s} = 8$ TeV. The resulting signal strengths $\mu_{t\bar{t}h,\gamma\gamma}^{\text{CMS}(lep)}$ and $\mu_{t\bar{t}h,\gamma\gamma}^{\text{CMS}(had)}$ are also shown. Note that the CMS cuts $N(j) \geq 4, N(b) \geq 1$ for $\gamma\gamma$ hadronic channel is not strong enough to separate $t\bar{t}h$ from thX processes.

LHC-8		With CMS Analysis Cuts			
	$C_t^S = 1$	$C_t^S = -1$	$C_t^S = 1.5$	$C_t^S = -1.5$	
Leptonic Selection					
Efficiency of $t\bar{t}h$	1.13e-5				
ϵ_1	1	1.91	0.67	2.31	
ϵ_2	0.03	0.05	0.01	0.05	
ϵ_3	0.11	0.24	0.05	0.25	
ϵ_4	0.57	2.03	0.56	1.91	
$\mu_{t\bar{t}h,\gamma\gamma}^{\text{CMS}(lep)}$	1.03	2.53	1.54	6.19	
Hadronic Selection					
Efficiency of $t\bar{t}h$	1.47e-4				
ϵ_1	1	2.34	0.71	2.43	
ϵ_2	0.44	0.10	0.29	1.27	
ϵ_3	1.40	3.82	0.99	3.96	
ϵ_4	0.52	1.53	0.36	1.72	
$\mu_{t\bar{t}h,\gamma\gamma}^{\text{CMS}(had)}$	1.04	3.45	1.61	7.48	
Combined $\mu_{t\bar{t}h,\gamma\gamma}^{\text{CMS}}$	1.15	6.96	1.79	13.3	

the category $\gamma\gamma$, we would like to make some remarks on a few noticeable aspects from the ATLAS $t\bar{t}h$ search. It has been shown that there was no significant excess over the background in the $h \rightarrow \gamma\gamma$ mode, and thus the 95% CL upper limit is set at $6.7 \times \sigma_{\text{SM}}(t\bar{t}h)$. Especially, ATLAS also took into account the dependence of the $t\bar{t}h$ and thX cross sections as well as the branching ratio $B(h \rightarrow \gamma\gamma)$ on the top-Yukawa coupling. The ATLAS $t\bar{t}h$ search sets the lower and upper limits on C_t^S : $-1.3 \leq C_t^S \leq 8.0$ at 95% CL.

In Table VII, we show the \mathcal{D} -dependent detection efficiency ratios $\epsilon_{1,2,3,4}$ with the CMS cuts in the hadronic-selection (upper) and leptonic-selection (lower) subcategories for $C_t^S =$

TABLE VIII. Category $\gamma\gamma$: The same as Table VII with the ATLAS cuts.

LHC-8	With ATLAS Analysis Cuts			
	$C_t^S = 1$	$C_t^S = -1$	$C_t^S = 1.5$	$C_t^S = -1.5$
Leptonic Selection				
Efficiency of $t\bar{t}h$	8.15e-6			
ϵ_1	1	1.64	0.65	3.00
ϵ_2	0.03	0.20	0.07	0.14
ϵ_3	0.14	0.26	0.04	0.28
ϵ_4	0.82	1.74	0.71	1.08
$\mu_{t\bar{t}h,\gamma\gamma}^{\text{ATLAS}}(lep)$	1.04	2.50	1.53	7.77
Hadronic Selection				
Efficiency of $t\bar{t}h$	1.06e-4			
ϵ_1	1	2.38	0.69	2.46
ϵ_2	0.05	0.11	0.03	0.17
ϵ_3	0.39	1.09	0.30	1.15
ϵ_4	0.39	1.15	0.26	1.20
$\mu_{t\bar{t}h,\gamma\gamma}^{\text{ATLAS}}(had)$	1.04	3.45	1.61	7.48
Combined $\mu_{t\bar{t}h,\gamma\gamma}^{\text{ATLAS}}$	1.04	3.38	1.61	7.50

$\pm 1, \pm 1.5$. By using the cross section ratios given in Table IV, one can obtain the CMS $t\bar{t}h$ signal strengths $\mu_{t\bar{t}h,\gamma\gamma}^{\text{CMS}}(lep)$ and $\mu_{t\bar{t}h,\gamma\gamma}^{\text{CMS}}(had)$ using Eq. (12). We observe that $\mu_{t\bar{t}h,\gamma\gamma}^{\text{CMS}}(lep) > 2$ (6) and $\mu_{t\bar{t}h,\gamma\gamma}^{\text{CMS}}(had) > 3$ (7) for $C_t^S = -1$ (-1.5). Also presented is the combined signal strength $\mu_{t\bar{t}h,\gamma\gamma}^{\text{CMS}}$ which is obtained by counting the event rates by combining the hadronic and leptonic selections. Similarly, in Table VIII, we show the \mathcal{D} -dependent detection efficiency ratios $\epsilon_{1,2,3,4}$ with the ATLAS cuts and the signal strengths $\mu_{t\bar{t}h,\gamma\gamma}^{\text{ATLAS}}(lep)$, $\mu_{t\bar{t}h,\gamma\gamma}^{\text{ATLAS}}(had)$, and $\mu_{t\bar{t}h,\gamma\gamma}^{\text{ATLAS}}$. Similar observations can be made as in the CMS case.

Finally, in Fig. 6, we show the accumulative combined signal strengths $\mu_{t\bar{t}h,\gamma\gamma}^{\text{ATLAS}}$ (left) and $\mu_{t\bar{t}h,\gamma\gamma}^{\text{CMS}}$ (right) at $\sqrt{s} = 8$ TeV by stacking the various thX contributions on the $t\bar{t}h$ one for $C_t^S = +1, -1, +1.5, -1.5$ from left to right. The grey columns in the center without C_t^S value represent the current 8 TeV LHC data, see Table I.

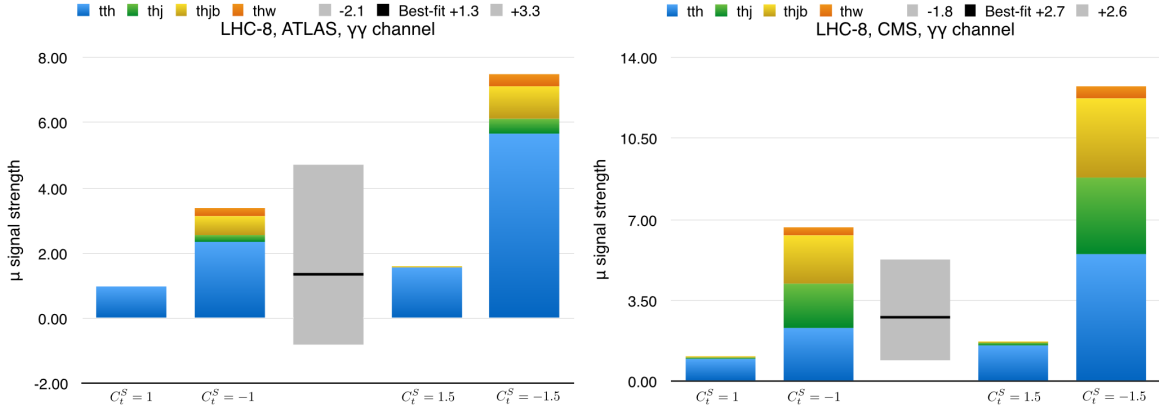


FIG. 6. Category $\gamma\gamma$: Accumulated signal strengths $\mu_{t\bar{t}h,\gamma\gamma}^{\text{ATLAS}}$ (left) and $\mu_{t\bar{t}h,\gamma\gamma}^{\text{CMS}}$ (lower right) at LHC-8 obtained by stacking the various thX contributions on the $t\bar{t}h$ one for $C_t^S = +1, -1, +1.5, -1.5$ from left to right. The grey columns in the center represent the current 8 TeV LHC data from Table I.

C. Category $b\bar{b}$ for $h \rightarrow b\bar{b}$

In the category $b\bar{b}$ for $h \rightarrow b\bar{b}$, we consider the semileptonic and leptonic decay modes of the top-quark pair which leads to the two subcategories of *single lepton* (1ℓ) and *dilepton* (2ℓ). The CMS preselection cuts shown in Table II and the ATLAS ones in Table III are first applied. And we further impose $P_{T_j} > 40$ GeV for the leading 3 jets in the single-lepton subcategory. In the dilepton subcategory, we select the events with exactly two oppositely charged leptons e^+e^- , $e^\pm\mu^\mp$, $\mu^+\mu^-$ with $P_{T_{l_1}} > 25$ GeV and $P_{T_{l_2}} > 15$ GeV. For $e^\pm\mu^\mp$ events, we further require H_T , scalar sum of transverse momenta of leptons and jets, to be larger than 130 GeV. For e^+e^- and $\mu^+\mu^-$ events, we impose two more conditions: (i) more than 2 b -jets and $M_{ll} > 15$ GeV to reduce the J/Ψ background and (ii) exactly 2 b -jets, $M_{ll} > 60$ GeV to remove the events in the low-mass region with large error bars, and $|M_{ll} - M_Z| > 8$ GeV to veto the Z background. We then combine these selections to complete the dilepton selection.

In Table IX, we show the \mathcal{D} -dependent detection efficiency ratios $\epsilon_{1,2,3,4}$ with the CMS cuts in the single-lepton (upper) and dilepton (lower) subcategories for $C_t^S = \pm 1, \pm 1.5$. By using the cross section ratios given in Table IV, one can obtain the CMS $t\bar{t}h$ signal strengths $\mu_{t\bar{t}h,b\bar{b}(1\ell)}^{\text{CMS}}$ and $\mu_{t\bar{t}h,b\bar{b}(2\ell)}^{\text{CMS}}$ using Eq. (12). We observe that $\mu_{t\bar{t}h,b\bar{b}(1\ell)}^{\text{CMS}} > 2$ for $C_t^S = -1, \pm 1.5$ and $\mu_{t\bar{t}h,b\bar{b}(2\ell)}^{\text{CMS}} > 2$ for $C_t^S = \pm 1.5$. The combined signal strength $\mu_{t\bar{t}h,b\bar{b}}^{\text{CMS}} > 2$ for $C_t^S = -1, \pm 1.5$.

TABLE IX. Category $b\bar{b}$: The \mathcal{D} -dependent detection efficiency ratios ϵ_i 's defined in Eq. (10) with the CMS cuts for the category $b\bar{b}$ taking $C_t^S = \pm 1, \pm 1.5$ and $\sqrt{s} = 8$ TeV. The resulting signal strengths $\mu_{t\bar{t}h, b\bar{b}(1\ell)}^{\text{CMS}}$ and $\mu_{t\bar{t}h, b\bar{b}(2\ell)}^{\text{CMS}}$ and the combined one $\mu_{t\bar{t}h, b\bar{b}}^{\text{CMS}}$ are also shown.

LHC-8		With CMS Analysis Cuts			
	$C_t^S = 1$	$C_t^S = -1$	$C_t^S = 1.5$	$C_t^S = -1.5$	
Single Lepton					
Efficiency of $t\bar{t}h$	1.17e-1				
ϵ_1	1	1	0.98	1	
ϵ_2	0.39	0.42	0.38	0.41	
ϵ_3	0.67	0.69	0.69	0.70	
ϵ_4	0.81	0.89	0.82	0.89	
$\mu_{t\bar{t}h, b\bar{b}(1\ell)}^{\text{CMS}}$	1.12	2.37	2.44	4.34	
Dilepton					
Efficiency of $t\bar{t}h$	2.03e-2				
ϵ_1	1	1.09	1.04	0.99	
ϵ_2	0.14	0.18	0.17	0.17	
ϵ_3	0.33	0.37	0.33	0.36	
ϵ_4	0.73	0.87	0.77	0.80	
$\mu_{t\bar{t}h, b\bar{b}(2\ell)}^{\text{CMS}}$	1.06	1.81	2.47	3.29	
Combined $\mu_{t\bar{t}h, b\bar{b}}^{\text{CMS}}$	1.11	2.29	2.44	4.19	

Similarly, in Table X, we show the \mathcal{D} -dependent detection efficiency ratios $\epsilon_{1,2,3,4}$ with the ATLAS cuts and the signal strengths $\mu_{t\bar{t}h, b\bar{b}(1\ell)}^{\text{ATLAS}}$, $\mu_{t\bar{t}h, b\bar{b}(2\ell)}^{\text{ATLAS}}$, and $\mu_{t\bar{t}h, b\bar{b}}^{\text{ATLAS}}$. Similar observations can be made as in the CMS case.

Finally, we show in Fig. 7 the accumulative combined signal strengths $\mu_{t\bar{t}h, b\bar{b}}^{\text{ATLAS}}$ (left) and $\mu_{t\bar{t}h, b}^{\text{CMS}}$ (right) at $\sqrt{s} = 8$ TeV by stacking the various thX contributions on the $t\bar{t}h$ one for $C_t^S = +1, -1, +1.5, -1.5$ from left to right. The grey columns in the center without C_t^S value represent the current 8 TeV LHC data, see Table I.

TABLE X. Category $b\bar{b}$: The same as Table IX but with the ATLAS cuts.

LHC-8		With ATLAS Analysis Cuts			
	$C_t^S = 1$	$C_t^S = -1$	$C_t^S = 1.5$	$C_t^S = -1.5$	
Single Lepton					
Efficiency of $t\bar{t}h$	1.19e-1				
ϵ_1	1	1.01	0.99	0.99	
ϵ_2	0.36	0.40	0.40	0.42	
ϵ_3	0.66	0.68	0.69	0.69	
ϵ_4	0.78	0.88	0.80	0.88	
$\mu_{t\bar{t}h, b\bar{b}(1\ell)}^{\text{ATLAS}}$	1.11	2.33	2.46	4.34	
Dilepton					
Efficiency of $t\bar{t}h$	1.57e-2				
ϵ_1	1	1.02	1.07	0.95	
ϵ_2	0.07	0.08	0.06	0.08	
ϵ_3	0.11	0.13	0.11	0.11	
ϵ_4	0.86	0.86	0.86	0.86	
$\mu_{t\bar{t}h, b\bar{b}(2\ell)}^{\text{ATLAS}}$	1.04	1.41	2.50	2.75	
Combined $\mu_{t\bar{t}h, b\bar{b}}^{\text{ATLAS}}$	1.11	2.22	2.46	4.15	

IV. DISENTANGLING thX FROM $t\bar{t}h$

In this section, we show kinematic distributions for the $t\bar{t}h$ and for thX processes in the presence of anomalous top-Yukawa coupling in an attempt to disentangle thX production from $t\bar{t}h$ one using specific selection cuts. We focus on the $h \rightarrow \gamma\gamma$ channel at the LHC with $\sqrt{s} = 13$ TeV (LHC-13) adopting the Delphes ATLAS fast detector simulation. We closely follow the analysis in a previous work [11]. Here we use the thj process for illustration while the other thX processes have similar features.

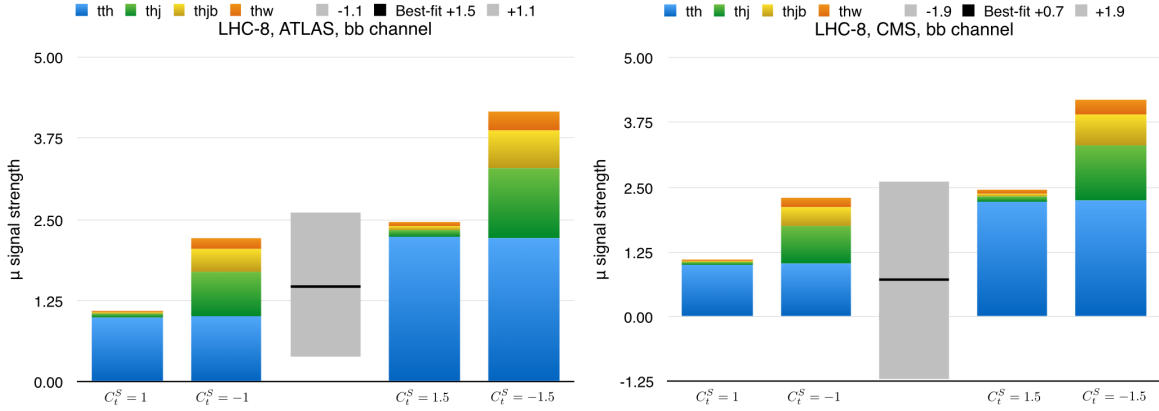


FIG. 7. Category $b\bar{b}$: Accumulated signal strengths $\mu_{t\bar{t}h,bb}^{\text{ATLAS}}$ (left) and $\mu_{t\bar{t}h,bb}^{\text{CMS}}$ (lower right) at LHC-8 obtained by stacking the various thX contributions on the $t\bar{t}h$ one for $C_t^S = +1, -1, +1.5, -1.5$ from left to right. The grey columns in the center represent the current 8 TeV LHC data from Table I.

TABLE XI. The cross-section ratios $R(t\bar{t}h)$ and $R(thX)$ with $X = j, jb, W$ defined in Eq. (9). We are taking $\sqrt{s} = 13$ TeV (LHC-13) and $C_t^S = \pm 1, \pm 1.5$.

LHC-13	With ATLAS Analysis Cuts			
	$C_t^S = 1$	$C_t^S = -1$	$C_t^S = 1.5$	$C_t^S = -1.5$
Cross Section of $t\bar{t}h$ (pb)	0.52			
$R(t\bar{t}h)$	1	1	2.26	2.26
$R(thj)$	0.16	1.72	0.29	2.65
$R(thjb)$	4.96e-2	0.57	8.96e-2	0.89
$R(thW)$	4.4e-2	0.29	9.39e-2	0.46

A. LHC-13

In Table XI, we show the cross sections ratios $R(t\bar{t}h)$ and $R(thX)$ with $X = j, jb, W$ at the 13 TeV LHC taking $C_t^S = \pm 1$ and ± 1.5 . Comparing the ratios at $\sqrt{s} = 8$ TeV presented in Table IV, we observe the LHC-13 ratios are more or less similar to the LHC-8 ones.

We show the p_{T_γ} and η_j distributions for the $t\bar{t}h$ and thX processes in Fig. 8 and Fig. 9, respectively, taking $C_t^S = \pm 1, \pm 1.5$. With $C_t^S \neq 1$, the p_{T_γ} distribution of the thX process, especially, that of the thW process becomes harder relative to the $t\bar{t}h$ distribution. In the

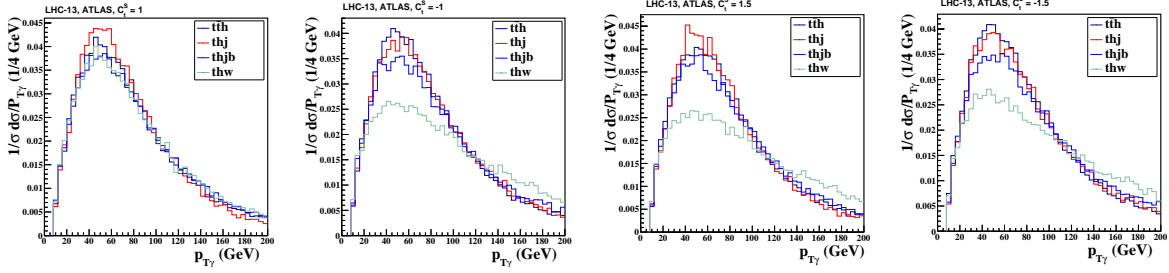


FIG. 8. The p_{T_γ} distributions for the $t\bar{t}h$ and thX processes in the $h \rightarrow \gamma\gamma$ channel at LHC-13 taking $C_t^S = +1, -1, +1.5, -1.5$ from left to right. We use the Delphes ATLAS template for detector simulations.

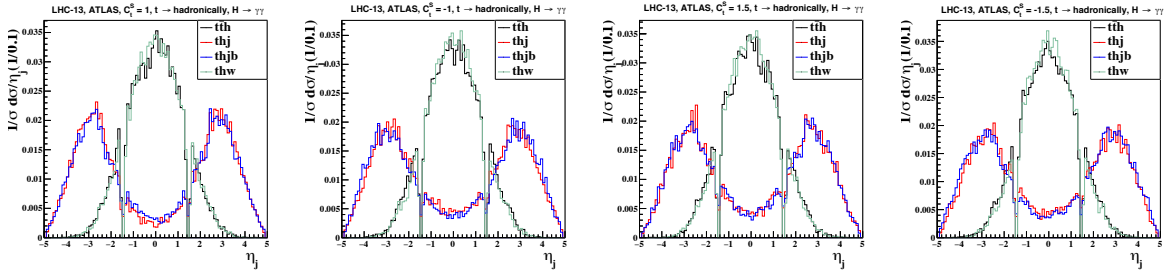


FIG. 9. The same as in Fig. 8 but for the η_j distributions.

η_j distributions, the thj and $thjb$ processes have more forward pseudorapidity. We therefore come up with a set of selection cuts summarized in Table XII, in which we order the jets according to their energy since most of the time the forward jet is most energetic one. It is in general correctly chosen as shown in the η_j distribution. Note that we require to tag one forward jet and apply the Higgs-mass window cut on the diphoton invariant mass $M_{\gamma\gamma}$.

TABLE XII. Selection cuts to disentangle thX from $t\bar{t}h$. The Delphes ATLAS template is used.

LHC-13	ATLAS Analysis Cuts, $h \rightarrow \gamma\gamma$
Basic cuts :	$\Delta R_{ij} > 0.4$ with i, j denoting b, j and l
	$P_{Tb} > 25\text{GeV}, \eta_b < 2.5, P_{Tl} > 25\text{GeV}, \eta_l < 2.5, P_{Tj} > 25\text{GeV}, \eta_j < 4.7$
# of γ & Higgs mass window cuts :	$N(\gamma) = 2, M_{\gamma\gamma} - m_h < 5\text{GeV}$
$t\bar{t}h$ search	$ \eta_j < 2.5$
thj search	Forward jet-tag : $2.5 < \eta_j < 4.7$
$t \rightarrow$ semileptonically & leptonically :	$N(e \text{ or } \mu)=1, E_T^{miss} > 20\text{GeV},$ Invariant Mass cuts for top decay product : $M_{bl} < 200\text{GeV}$ $t\bar{t}h$ search : $N(j) \geq 2, N(b) \geq 1$ thj search : $N(j) \leq 3, N(b) \leq 2$
$t \rightarrow$ hadronically :	$N(e \text{ or } \mu)=0, \text{Invariant Mass cuts for top decay product : } M_{bj_1j_2} < 300\text{GeV}$ $t\bar{t}h$ search : $N(j) \geq 6, N(b) \geq 2$ thj search : $N(j) \leq 5, N(b) \leq 2$

The accumulated thj signal strength $\mu(thj)$ ⁶ is shown in the left panel of Fig. 10 with $C_t^S = \pm 1, \pm 1.5$. To obtain the signal strength $\mu(thj)$ in the $h \rightarrow \gamma\gamma$ decay at LHC-13, we impose the thj -specific cuts listed in Table XII. In the right panel of Fig. 10, we show the accumulated $t\bar{t}h$ signal strength $\mu(t\bar{t}h)$ obtained by using the $t\bar{t}h$ -specific cuts in the same Table. We observe that $\mu(thj)$ (left) is dominated by thj (green) for the negative values of C_t^S , implying that our thj -specific cuts are working very efficiently when the thj production cross section is much enhanced with $R(thj) > 1$. On the other hand, $\mu(t\bar{t}h)$ (right) is dominated by $t\bar{t}h$ (blue) independently of C_t^S and we observe that our $t\bar{t}h$ -specific cuts are working reasonably well as in the LHC-8 case (the left panel of Fig. 6). We can further draw a few observations from Fig. 10 as follows.

1. Both of the signal strengths depend on the sign of the top-Yukawa coupling even for $C_t^S = \pm 1$. This is because the branching ratio $B(h \rightarrow \gamma\gamma)$ increases when C_t^S becomes negative. For example, just $t\bar{t}h$ alone can increase the signal strength $\mu(t\bar{t}h)$ to 2.5.

⁶ Similarly as $\mu(t\bar{t}h)$ given by Eq. (8), the signal strength $\mu(thj)$ is

$$\mu(thj) = \frac{\eta_1 \sigma(t\bar{t}h) B(t\bar{t}h \rightarrow \mathcal{D}) + \sum_{X=j, j_b, W} \eta_X \sigma(thX) B(thX \rightarrow \mathcal{D})}{\eta_j^{\text{SM}} \sigma(thj)_{\text{SM}} B(thj \rightarrow \mathcal{D})_{\text{SM}}}.$$

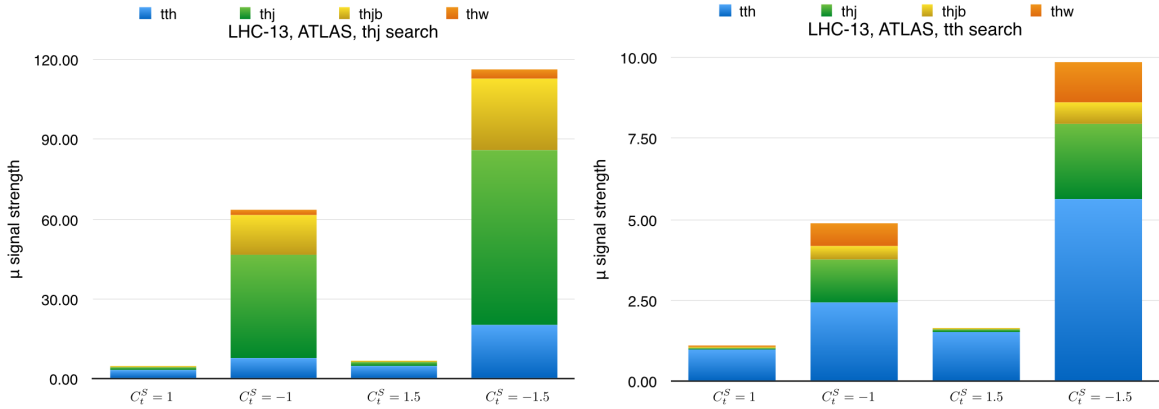


FIG. 10. Accumulated signal strengths $\mu(thj)$ (left) and $\mu(t\bar{t}h)$ (right) at LHC-13 obtained by stacking the various thX contributions on the $t\bar{t}h$ one for $C_t^S = +1, -1, +1.5, -1.5$ from left to right. We use the Delphes ATLAS template for detector simulations.

2. When the experiment is targeting the $t\bar{t}h$ production using the $t\bar{t}h$ -specific cuts, there are contaminations from the thX processes. For positive C_t^S , the thX contaminations are small. But, for negative C_t^S , they can be as large as the $t\bar{t}h$ signals. For $C_t^S = -1$, for example, $\mu(t\bar{t}h) = 5$ and only half of which comes from $t\bar{t}h$.
3. From the left panel, we can see that the thX processes dominate the signal strength $\mu(thj)$ for negative C_t^S , which means that the thj -specific selection cuts we employed indeed can single out the thj process from the $t\bar{t}h$ one.

V. CONCLUSIONS

The same-sign dilepton channel excess in $t\bar{t}h$ production has caught the attention of many people. Indeed, the current data on $t\bar{t}h$ production also showed excesses at some level in other channels. Usually, the associated Higgs production with a single top quark dubbed as thX with $X = j, jb, W$ makes only small contributions to the overall experimental signal strength of $\mu(t\bar{t}h)$. In this work, however, we have demonstrated explicitly that the thX processes can significantly increase the experimentally measured signal strength $\mu(t\bar{t}h)$ when the relative sign of the top-Yukawa coupling to the gauge-Higgs coupling is reversed. The signal strengths can be as large as 2–4 in the category Leptons for $h \rightarrow$ multileptons, 7–13 in the category $\gamma\gamma$ for $h \rightarrow \gamma\gamma$, and 2–4 in the category $b\bar{b}$ for $h \rightarrow b\bar{b}$. We note that all

go in the right direction to match the current 8-TeV data on the excesses observed at the LHC.

When more data are collected at $\sqrt{s} = 13$ TeV, we can choose more specific cuts to single out the thX processes, which can effectively determine the size and the sign of the top-Yukawa coupling.

We offer the following comments on our findings.

1. When the top-Yukawa coupling is kept at the SM value, i.e. $C_t^S = 1$, the contamination from all the thX processes is small, only about 5 – 15%, and that can be regarded as a sort of small higher-order corrections.
2. However, when the sign of the top-Yukawa coupling is reversed, i.e. $C_t^S = -1$, the thX contributions are significantly enhanced. And the resulting signal strengths can be as large as 1.5 – 2.4 (category Leptons), 2.5 – 7.0 (category $\gamma\gamma$), and 1.4 – 2.4 (category $b\bar{b}$), explaining the experimental excesses shown in Table I.
3. When C_t^S is further negative, say -1.5 , the resulting signal strength $\mu(t\bar{t}h)$ further increases to 3.0 – 4.5 (category Leptons), 6.2 – 13 (category $\gamma\gamma$), and 2.8 – 4.3 (category $b\bar{b}$).
4. The dominant thX processes are thj and $thjb$, both of which contain a very forward energetic jet. Also, as shown in Fig. 8 the thW process has a harder p_T photon. Therefore, we successfully come up with a set of selection cuts to single out the thX processes from the $t\bar{t}h$ process. It has been shown clearly in the left panel of Fig. 10.

Note added: At the last stage of this work, we came across a conference proceedings [22] from CMS on $t\bar{t}h$ production at $\sqrt{s} = 13$ TeV, at which the signal strength for $t\bar{t}h$ is closer to the SM value.

ACKNOWLEDGMENT

This work was supported by the MoST of Taiwan under Grants No. 102-2112-M-007-015-MY3.

-
- [1] G. Aad *et al.* [ATLAS Collaboration], Phys. Lett. B **716**, 1 (2012) [arXiv:1207.7214 [hep-ex]].
- [2] S. Chatrchyan *et al.* [CMS Collaboration], Phys. Lett. B **716**, 30 (2012) [arXiv:1207.7235 [hep-ex]].
- [3] See for example, K. Cheung, J. S. Lee and P. -Y. Tseng, JHEP **1305**, 134 (2013) [arXiv:1302.3794 [hep-ph]].
K. Cheung, J. S. Lee and P. Y. Tseng, Phys. Rev. D **90**, 095009 (2014) doi:10.1103/PhysRevD.90.095009 [arXiv:1407.8236 [hep-ph]].
- [4] P. W. Higgs, Phys. Rev. Lett. **13**, 508 (1964); F. Englert and R. Brout, Phys. Rev. Lett. **13**, 321 (1964); G. S. Guralnik, C. R. Hagen and T. W. B. Kibble, Phys. Rev. Lett. **13**, 585 (1964).
- [5] ATLAS Coll., "Measurements of the Higgs boson production and decay rates and couplings using pp collision data at sqrt(s)=7 and 8 TeV in the ATLAS experiment", ATLAS-CONF-2015-007 (March 2015); V. Khachatryan *et al.* [CMS Collaboration], Eur. Phys. J. C **75**, no. 5, 212 (2015) doi:10.1140/epjc/s10052-015-3351-7 [arXiv:1412.8662 [hep-ex]].
- [6] G. Aad *et al.* [ATLAS Collaboration], JHEP **1510**, 150 (2015) doi:10.1007/JHEP10(2015)150 [arXiv:1504.04605 [hep-ex]].
- [7] V. Khachatryan *et al.* [CMS Collaboration], JHEP **1409**, 087 (2014) [JHEP **1410**, 106 (2014)] doi:10.1007/JHEP09(2014)087, 10.1007/JHEP10(2014)106 [arXiv:1408.1682 [hep-ex]].
- [8] S. Chatrchyan *et al.* [CMS Collaboration], JHEP **1401**, 163 (2014) [JHEP **1501**, 014 (2015)] doi:10.1007/JHEP01(2015)014, 10.1007/JHEP01(2014)163 [arXiv:1311.6736, arXiv:1311.6736 [hep-ex]].
G. Aad *et al.* [ATLAS Collaboration], JHEP **1406**, 035 (2014) doi:10.1007/JHEP06(2014)035 [arXiv:1404.2500 [hep-ex]].
G. Aad *et al.* [ATLAS Collaboration], Phys. Lett. B **749**, 519 (2015) doi:10.1016/j.physletb.2015.07.079 [arXiv:1506.05988 [hep-ex]].

- G. Aad *et al.* [ATLAS Collaboration], JHEP **1511**, 172 (2015) doi:10.1007/JHEP11(2015)172 [arXiv:1509.05276 [hep-ex]].
- V. Khachatryan *et al.* [CMS Collaboration], arXiv:1510.01131 [hep-ex].
- [9] B. Bhattacharjee, S. Chakraborty and S. Mukherjee, arXiv:1505.02688 [hep-ph].
- P. Huang, A. Ismail, I. Low and C. E. M. Wagner, Phys. Rev. D **92**, no. 7, 075035 (2015) doi:10.1103/PhysRevD.92.075035 [arXiv:1507.01601 [hep-ph]].
- C. R. Chen, H. C. Cheng and I. Low, arXiv:1511.01452 [hep-ph].
- [10] G. Aad *et al.* [ATLAS Collaboration], Phys. Lett. B **749**, 519 (2015) doi:10.1016/j.physletb.2015.07.079 [arXiv:1506.05988 [hep-ex]].
- [11] J. Chang, K. Cheung, J. S. Lee and C. T. Lu, JHEP **1405**, 062 (2014) doi:10.1007/JHEP05(2014)062 [arXiv:1403.2053 [hep-ph]].
- [12] T. M. P. Tait and C.-P. Yuan, Phys. Rev. D **63**, 014018 (2000) doi:10.1103/PhysRevD.63.014018 [hep-ph/0007298].
- V. Barger, M. McCaskey and G. Shaughnessy, Phys. Rev. D **81**, 034020 (2010) [arXiv:0911.1556 [hep-ph]].
- S. Biswas, E. Gabrielli and B. Mele, JHEP **1301**, 088 (2013) [arXiv:1211.0499 [hep-ph]]; S. Biswas, E. Gabrielli, F. Margaroli and B. Mele, JHEP **07**, 073 (2013) [arXiv:1304.1822 [hep-ph]].
- M. Farina, C. Grojean, F. Maltoni, E. Salvioni and A. Thamm, JHEP **1305**, 022 (2013) [arXiv:1211.3736 [hep-ph]].
- P. Agrawal, S. Mitra and A. Shivaji, arXiv:1211.4362 [hep-ph].
- J. Ellis, D. S. Hwang, K. Sakurai and M. Takeuchi, arXiv:1312.5736 [hep-ph].
- C. Englert and E. Re, arXiv:1402.0445 [hep-ph].
- A. Kobakhidze, L. Wu and J. Yue, JHEP **1410**, 100 (2014) doi:10.1007/JHEP10(2014)100 [arXiv:1406.1961 [hep-ph]].
- J. Yue, Phys. Lett. B **744**, 131 (2015) doi:10.1016/j.physletb.2015.03.044 [arXiv:1410.2701 [hep-ph]].
- F. Demartin, F. Maltoni, K. Mawatari and M. Zaro, Eur. Phys. J. C **75**, no. 6, 267 (2015) doi:10.1140/epjc/s10052-015-3475-9 [arXiv:1504.00611 [hep-ph]].
- [13] J. S. Lee, A. Pilaftsis, M. S. Carena, S. Y. Choi, M. Drees, J. R. Ellis and C. E. M. Wagner, Comput. Phys. Commun. **156** (2004) 283 [hep-ph/0307377].

- [14] G. Aad *et al.* [ATLAS Collaboration], Phys. Lett. B **740**, 222 (2015) doi:10.1016/j.physletb.2014.11.049 [arXiv:1409.3122 [hep-ex]].
- [15] G. Aad *et al.* [ATLAS Collaboration], Eur. Phys. J. C **75**, no. 7, 349 (2015) doi:10.1140/epjc/s10052-015-3543-1 [arXiv:1503.05066 [hep-ex]].
- [16] J. Alwall *et al.*, JHEP **1407**, 079 (2014) doi:10.1007/JHEP07(2014)079 [arXiv:1405.0301 [hep-ph]].
- [17] T. Sjostrand, S. Mrenna and P. Z. Skands, Comput. Phys. Commun. **178**, 852 (2008) doi:10.1016/j.cpc.2008.01.036 [arXiv:0710.3820 [hep-ph]].
- [18] J. de Favereau *et al.* [DELPHES 3 Collaboration], JHEP **1402**, 057 (2014) [arXiv:1307.6346 [hep-ex]].
- [19] V. Khachatryan *et al.* [CMS Collaboration], Phys. Lett. B **749**, 337 (2015) doi:10.1016/j.physletb.2015.07.053 [arXiv:1502.07400 [hep-ex]].
- [20] A. Djouadi, J. Kalinowski, M. Spira [arXiv:9704448 [hep-ph]].
- [21] ATLAS Collaboration, Calibration of the performance of b-tagging for c and light-flavour jets in the 2012 ATLAS data, Tech. Rep. ATLAS- CONF-2014-046 (July 2014).
- [22] CMS Collaboration, CMS PAS HIG-15-008, “Search for $t\bar{t}H$ production in multilepton final states at $\sqrt{s} = 13$ TeV” (2016/03/23); CMS Collaboration, CMS PAS HIG-16-004, “Search for $t\bar{t}H$ production in the $H \rightarrow b\bar{b}$ decay channel with $\sqrt{s} = 13$ TeV pp collisions at the CMS experiment” (2016/03/16).